Structural Investigation of Combustion Synthesized Cu/CeO_2 Catalysts by EXAFS and Other Physical Techniques: Formation of a $Ce_{1-x}Cu_xO_{2-\delta}$ Solid Solution

Parthasarathi Bera,[†] K. R. Priolkar,[‡] P. R. Sarode,[‡] M. S. Hegde,*[,†] S. Emura,[§] R. Kumashiro,[||] and N. P. Lalla[⊥]

Solid State and Structural Chemistry Unit, Indian Institute of Science, Bangalore-560012, India, Department of Physics, Goa University, Goa-403206, India, Institute of Scientific and Industrial Research, Osaka University, Mihoga-oka 8-1, Ibaraki, Osaka 567-0047, Japan, Research Laboratory for Surface Science, Faculty of Science, Okayama University, Tsushima-naka, Okayama 700-8530, Japan, and Inter University Consortium, University Campus, Indore-452017, India

Received March 13, 2002. Revised Manuscript Received June 4, 2002

The structure and chemical environment of Cu in Cu/CeO_2 catalysts synthesized by the solution combustion method have been investigated by X-ray diffraction (XRD), transmission electron microscopy (TEM), electron paramagnetic resonance (EPR) spectroscopy, X-ray photoelectron spectroscopy (XPS), cyclic voltammetry (CV), and extended X-ray fine structure (EXAFS) spectroscopy. High-resolution XRD studies of 3 and 5 atom % Cu/CeO_2 do not show CuO lines in their respective patterns. The structure could be refined for the composition $Ce_{1-x}Cu_xO_{2-\delta}$ ($x = 0.03$ and 0.05; $\delta \sim 0.13$ and 0.16) in the fluorite structure with 5−8% oxide ion vacancy. High-resolution TEM did not show CuO particles in 5 atom % Cu/CeO_2. EPR as well as XPS studies confirm the presence of Cu^{2+} species in the CeO_2 matrix. Redox potentials of Cu species in the CeO_2 matrix are lower than those in CuO. EXAFS investigations of these catalysts show an average coordination number of 3 around the Cu^{2+} ion in the first shell at a distance of 1.96 Å, indicating the O^{2-} ion vacancy around the Cu^{2+} ion. The Cu−O bond length also decreases compared to that in CuO. The second and third shell around the Cu^{2+} ion in the catalysts are attributed to $-Cu^{2+}-O^{2-}-Cu^{2+}-$ at 2.92 Å and $-Cu^{2+}-O^{2-}-Ce^{4+}-$ at the distance of 3.15 Å, respectively. The present results provide direct evidence for the formation of a $Ce_{1-x}Cu_xO_{2-\delta}$ type of solid solution phase having $-\square-Cu^{2+}-O-Ce^{4+}-$ kind of linkages.

Introduction

Copper based catalysts have recently attracted much attention in heterogeneous catalysis because of their high catalytic activities toward NO reduction and CO and hydrocarbon oxidation.[1−10] Cu/ZrO_2, Cu/CeO_2, Cu/TiO_2, and Cu^{2+} ion exchanged Y zeolite, mordenite, ZSM-5, and MFI-ferrisilicate have been found to be effective catalysts for selective catalytic reduction (SCR) of NO in the presence of O_2.[11−14] Liu and Robota[15] have predicted a cyclic redox mechanism involving Cu(I) and Cu(II) under oxygen rich conditions during SCR of NO by hydrocarbons over Cu−ZSM-5 catalyst. Huang and Wang[16] have suggested that Cu(I)) plays a major role in catalytic reduction of NO in the channels of ZSM-5. Therefore, it is important to understand the nature of the active Cu species of the supported Cu catalysts.

Flytzani-Stephanopoulos et al.[17] have shown complete CO oxidation over Cu/CeO_2 at 150 °C, whereas the same reaction occurs at much higher temperature over CeO_2. Harrison et al.[18,19] have demonstrated low-temperature

* Corresponding author. E-mail: mshegde@sscu.iisc.ernet.in (M.S.H.); partho@sscu.iisc.ernet.in (P.B.). Fax: +91-80-3601310.
[†] Indian Institute of Science.
[‡] Goa University.
[§] Osaka University.
[||] Okayama University.
[⊥] Inter University Consortium.

(1) Williamson, W. B.; Lunsford, J. H. *J. Phys. Chem.* **1976**, *80*, 2664.
(2) Rewick, R. T.; Wise, H. *J. Catal.* **1975**, *40*, 301.
(3) Blanco, J.; García de la Banda, J. F.; Avila, P.; Melo, F. *J. Phys. Chem.* **1986**, *90*, 4789.
(4) Iwamoto, M.; Yahiro, H.; Mizuno, N.; Zhang, W.; Mine, Y.; Furukawa, H.; Kagawa, S. *J. Phys. Chem.* **1992**, *96*, 9360.
(5) Komatsu, T.; Ogawa, T.; Yashima, T. *J. Phys. Chem.* **1995**, *99*, 13053.
(6) Trout, B. L.; Chakraborty, A. K.; Bell, A. T. *J. Phys. Chem.* **1996**, *100*, 17582.
(7) Li, Y.; Hall, W. K. *J. Phys. Chem.* **1990**, *94*, 6145.
(8) Dandekar, A.; Baker, R. T. K.; Vannice, M. A. *J. Catal.* **1999**, *183*, 131.
(9) Severino, F.; Lalne, J. *Ind. Eng. Chem. Prod. Res. Dev.* **1983**, *22*, 396.
(10) Martínez-Arias, A.; Fernández-García, M.; Soria, J.; Conesa, J. C. *J. Catal.* **1999**, *182*, 367.
(11) Okamoto, Y.; Gotoh, H.; Aritani, H.; Tanaka, T.; Yoshida, S. *J. Chem. Soc., Faraday Trans.* **1997**, *93*, 3879.
(12) Aritani, H.; Akasaka, N.; Tanaka, T.; Funabiki, T.; Yoshida, S.; Gotoh, H.; Okamoto, Y. *J. Chem. Soc., Faraday Trans.* **1996**, *92*, 2625.
(13) Komatsu, T.; Nunokawa, M.; Moon, I. S.; Takahara, T.; Namba, S.; Yashima, T. *J. Catal.* **1994**, *148*, 427.
(14) Komatsu, T.; Ueda, T.; Yashima, T. *J. Chem. Soc., Faraday Trans.* **1998**, *94*, 949.
(15) Liu, D.-J.; Robota, H. J. *J. Phys. Chem. B* **1999**, *103*, 2755.
(16) Huang, Y.-J.; Wang, H. P. *J. Phys. Chem. A* **1999**, *103*, 6514.
(17) Liu, W.; Flytzani-Stephanopoulos, M. *J. Catal.* **1995**, *153*, 304.

10.1021/cm0201706 CCC: $22.00
Published on Web 07/27/2002

CO oxidation over Cu/SnO_2 and Cu/CeO_2 prepared by coprecipitation and impregnation methods. They have shown that catalyst materials heated at 400 °C are most active. However, they could not isolate the active phase of Cu in Cu/CeO_2 and Cu/SnO_2 systems. Recently, we have reported NO reduction over combustion synthesized Cu/CeO_2 catalyst which works as an SCR catalyst in the lower temperature window of 150−350 °C.[20] Pure CeO_2 and Zr, Y, and Ca doped CeO_2 prepared by the same method show NO reduction at much higher temperature. Generally, it is believed that highly dispersed CuO over CeO_2 support is the active phase for high catalytic activity.[17,19] To gain an insight into the high catalytic activities of Cu/CeO_2 catalyst, it is essential to find the electronic and atomic structure of the material. We have investigated the structure of Cu/CeO_2 catalyst by high-resolution XRD, TEM, EPR, and XPS, and its catalytic activities are compared with those of CuO. H_2 uptake and CV measurements have also been carried out to study the redox properties of the catalyst. The local structure of Cu in the catalysts is investigated by extended X-ray absorption fine structure (EXAFS) spectroscopy. Here we report the structure of Cu/CeO_2 catalysts prepared by a combustion method and show that Cu forms a $Ce_{1-x}Cu_xO_{2-\delta}$ type of solid solution with oxide ion defects.

Experimental Section

Synthesis. The combustion mixture for the preparation of 3 atom % Cu/CeO_2 contained $(NH_4)_2Ce(NO_3)_6$ [E. Merck India Ltd., 99.9%], $Cu(CO_3)_2$, $Cu(OH)_2$ [Glaxo India Ltd., 99.9%], and $C_2H_6N_4O_2$ (oxalyldihydrazide) in the mole ratio 0.97:0.03:2.36. Oxalyldihydrazide (ODH) prepared from diethyl oxalate and hydrazine hydrate was used as the fuel. For the preparation of 3 atom % Cu/CeO_2, a borosilicate dish of 300 cm^3 capacity containing an aqueous redox mixture of stoichiometric amounts of $(NH_4)_2Ce(NO_3)_6$ (10 g), $Cu(CO_3)_2$, $Cu(OH)_2$ (0.135 g), and $C_2N_2O_4H_6$ (5.242 g) in 300 cm^3 of H_2O was introduced into a muffle furnace with temperature maintained at 350 °C. At the point of complete dehydration, the solution boiled with foaming and frothing and ignited to burn with a flame (∼1000 °C), yielding a voluminous oxide product within 5 min. The color of the sample is light green. 5 and 10 atom % Cu/CeO_2 samples were prepared in a similar way.

Catalytic Test. The catalytic reactions were carried out in a temperature programmed reaction system equipped with a quadrupole mass spectrometer QXK300 (VG Scientific Ltd., England) for product analysis in a packed bed tubular reactor. Typically, 0.1 g of the catalyst was loaded in a quartz tube reactor of 20 cm length and 6 mm diameter. The reactor was heated from 30 to 750 °C at a rate of 15 °C min^{-1}, and the sample temperature was measured with a fine chromel−alumel thermocouple immersed in the catalyst. The quartz tube was evacuated to 10^{-6} Torr. The gaseous products were sampled through a fine control leak valve to an ultrahigh vacuum (UHV) system housing the quadrupole mass spectrometer at 10^{-9} Torr. The gases were passed over the catalyst at a flow rate of 25 μmol s^{-1}. Accordingly, the gas hourly space velocity (GHSV) was 22 000 h^{-1}. The dynamic pressure of the gases was in the range of 10 Torr in the reaction system. All the masses were scanned every 10 s. At the end of the reaction, the intensity of each mass as a function of temperature (thermogram) was generated. The gases were obtained from Bhoruka Gases Ltd., Bangalore. Their purities were better than 99%, as analyzed by the quadrupole mass spectrometer.

H_2 Uptake Measurement. Hydrogen uptake studies were carried out in a temperature programmed reduction system by passing 10% H_2/Ar over 0.1 g of the catalyst in a quartz tube reactor of 20 cm length and 6 mm diameter. A thermal conducting detector (TCD) was employed to measure the volume of hydrogen utilized. The volume of hydrogen taken up by the catalyst is calibrated against pure CuO.

CV Measurement. Electrochemical studies of 5 atom % Cu/CeO_2 and CuO were carried out with a CH-660A electrochemical analyzer from CH Instruments using a three-electrode cell configuration. The working electrodes were made by mixing 65 wt. % graphite and 35 wt. % Cu based materials. The mixture was ground thoroughly, and 10 mm pellets of 1.5 mm thickness were made and subsequently mounted on a glass tube using conductive silver paint (Eltecks Corporation, India). Cu wire was used as the current collector. The electrode was polished to a shining mirror with fine grade emery (SiC) paper. The counter electrode used was a Pt foil, and a saturated calomel electrode (SCE) was used as the reference electrode. The electrolyte solution was 0.05 M sodium sulfate (Na_2SO_4). The electrolyte was degassed by bubbling with N_2 prior to the measurement. The electrodes were cycled from +1.6 to −0.8 V at different scan rates. All experiments were performed at ambient temperature (∼25 °C).

Characterization. XRD data of Cu/CeO_2 catalysts for Rietveld refinement were collected on a Rigaku-2000 diffractometer with a rotating anode using Cu Kα_1 radiation (1.540 59 Å) with a graphite-crystal monochromator. Data were obtained at a scan rate of 1° min^{-1} with 0.02° step size in the 2θ range 10−110°, and the structure was refined using the FullProf-98 program. The number of parameters refined simultaneously was 19. A JEOL JEM-200CX transmission electron microscope operated at 200 kV was used to carry out TEM studies.

Electron paramagnetic resonance (EPR) spectra of Cu/CeO_2 samples were recorded at 300 K using an E-Line X-band Varian EPR spectrometer at a frequency of 9.5 GHz. The magnetic field was modulated at 100 kHz. The g values were calculated by comparison with a DPPH (diphenyl picryl hydrazyl) sample ($g = 2.0036$).

X-ray photoelectron spectra of these materials were recorded in an ESCA-3 Mark II spectrometer (VG Scientific Ltd., England) using Al Kα radiation (1486.6 eV). Binding energies were calculated with respect to C(1s) at 285 eV. Binding energies were measured with a precision of ±0.2 eV.

EXAFS spectra of the Cu K-edge in catalysts and reference materials were recorded at room temperature in the transmission mode by using synchrotron radiation and employing a Si(111) double-crystal monochromator at the BL01B1 beamline of the Japan Synchrotron Radiation Research Institute (SPring-8), Japan. The monochromator was detuned slightly in order to reduce the amount of higher harmonics in the beam. The slit width of the monochromator exit was 1 mm vertical and 5 mm horizontal to ensure optimal resolution. During the measurement, the synchrotron was operated at an energy of 8 GeV and a current between 80 and 100 mA. The spectra were scanned in the range 8700−9900 eV for the Cu K-edge. The photon energy was calibrated for each scan with the first inflection point of the Cu K-edge in Cu metal foil. Both the incident (I_0) and transmitted (I) synchrotron beam intensities were measured simultaneously using an ionization chamber filled with 100% N_2 gas and a mixture of 50% Ar and 50% N_2 gases, respectively. The absorbers were made by sprinkling a fine powder of the sample uniformly on a Kapton tape and stacking a number of such layers together to achieve a desired thickness. The thickness of the absorber was adjusted such that $\Delta\mu_0 x$ was restricted to a value ≤ 1, where $\Delta\mu_0$ is the edge step in the absorption coefficient and x is the sample thickness.[21]

(18) Harrison, P. G.; Bailey, C.; Daniell, W.; Zhao, D.; Ball, I. K.; Goldfarb, D.; Lloyd, N. C.; Azelee, W. *Chem. Mater.* **1999**, *11*, 3643.
(19) Harrison, P. G.; Ball, I. K.; Azelee, W.; Daniell, W.; Goldfarb, D. *Chem. Mater.* **2000**, *12*, 3715.
(20) Bera, P.; Aruna, S. T.; Patil, K. C.; Hegde, M. S. *J. Catal.* **1999**, *186*, 36.
(21) Stern, E. A.; Kim, K. *Phys. Rev. B* **1981**, *23*, 3781.

EXAFS Data Analysis. EXAFS data have been analyzed using the UWXAFS program.[22] It uses the criteria of good background removal, optimization of the low-*R* portion of the EXAFS data, and Fourier transform to *R* space. Since the EXAFS function is a superposition of an unknown number of coordination shells, the Fourier transform (FT) technique gives information about the individual shells. The FT of the EXAFS function $\chi(k)$ to *R* space with k^1 weighting factor and Hanning window function (Dk1 and Dk2 = 0.1) has been performed in the 3−12 $Å^{-1}$ range, yielding a function $\Phi(R)$. The function $\Phi(R)$, where *R* is the distance from the absorber atom, is called a radial distribution function (RDF) or radial structure function (RSF). The value of the amplitude reduction factor (S_0^2) is deduced from Cu K-edge EXAFS of Cu metal with known crystal structural data.[23] The theoretical calculations of the backscattering amplitude and phase shift functions are obtained by using the FEFF (6.01) program.[24] The input files for the FEFF program are directly given from crystal structure information of atoms, such as lattice parameters, space group, and absorbing core. The experimental EXAFS data were fitted with the theoretical EXAFS function using the FEFFIT (2.5 d) program.[25] E_0 is one of the fitting parameters in the FEFFIT program. Initially, it was taken as the energy corresponding to the first inflection point in the derivative spectra of individual compounds. For Cu metal it was found to be 8979.4 eV within the error of 1 eV. After fitting, the final values of E_0 obtained are 8982.94, 8984.3, and 8986.24 eV for Cu metal, Cu_2O, and CuO, respectively. The goodness of fit has been judged by means of χ^2, reduced χ^2, and *R* factor discussed elsewhere.[26,27] From this analysis, structural parameters such as coordination numbers (*N*), bond distance (*R*), and Debye−Waller factor (σ) have been calculated.

Results

Catalytic Studies. The NO conversion rates for the NO + NH_3 and NO + CO reactions over 5 atom % Cu/CeO_2 and CuO as a function of temperature are shown in Figure 1. It is clear that complete NO conversion in the NO + NH_3 reaction occurs below 250 °C over 5 atom % Cu/CeO_2, producing N_2 and H_2O, whereas the same reaction takes place above 325 °C over CuO. During reaction over the catalyst, N_2O is formed at 200 °C to a little extent but decomposes at higher temperature. The reaction temperatures over the catalyst also follow the same trend for NO + CO and CO + O_2 reactions. The NO conversion in the NO + CO reaction over 5 atom % Cu/CeO_2 starts at 100 °C, and complete conversion is observed below 300 °C, giving N_2 and CO_2 as the products. On the other hand, CuO shows 100% NO conversion above 350 °C (Figure 1b). An increase in CO_2/N_2O (m/z = 44) concentration with a simultaneous decrease in NO (m/z = 30) concentration is taken as the measure of NO conversion. If N_2O is formed in the course of the reaction because of partial reduction of NO, it is not possible to distinguish between N_2O and CO_2, as the mass number of N_2O is the same as that of CO_2 (m/z = 44). Catalytic reduction of NO by NH_3 over the same 5 atom % Cu/CeO_2 catalyst shows a trace amount of N_2O formation (<5%) along with N_2 and H_2O in the temperature range 150−300 °C, and at higher temperature it decomposes and N_2 and H_2O are the only products. Since CO_2 is more stable than N_2O, the probability of CO_2 formation is higher than that of N_2O formation. Yet, the possibility of formation of N_2O to a little extent cannot be ruled out during the NO + CO reaction. Nonetheless, NO conversion at a lower temperature over 5 atom % Cu/CeO_2 prepared by a combustion method compared to CuO is clear from Figure 1. Similarly, complete CO conversion occurs over 5 atom % Cu/CeO_2 below 300 °C, whereas it occurs above 350 °C over CuO. These are only the typical catalytic reactions over 5 atom % Cu/CeO_2 to highlight higher catalytic activity at lower temperature, which can be attributed to the interaction of Cu species with CeO_2. These reactions occur at much higher temperatures over pure CeO_2. We have also observed an increase in light off temperature for the NO + NH_3 reaction with an increase in Cu content beyond 5 atom %. Therefore, 5 atom % Cu/CeO_2 is the optimum concentration, and the structure of this catalyst is important.

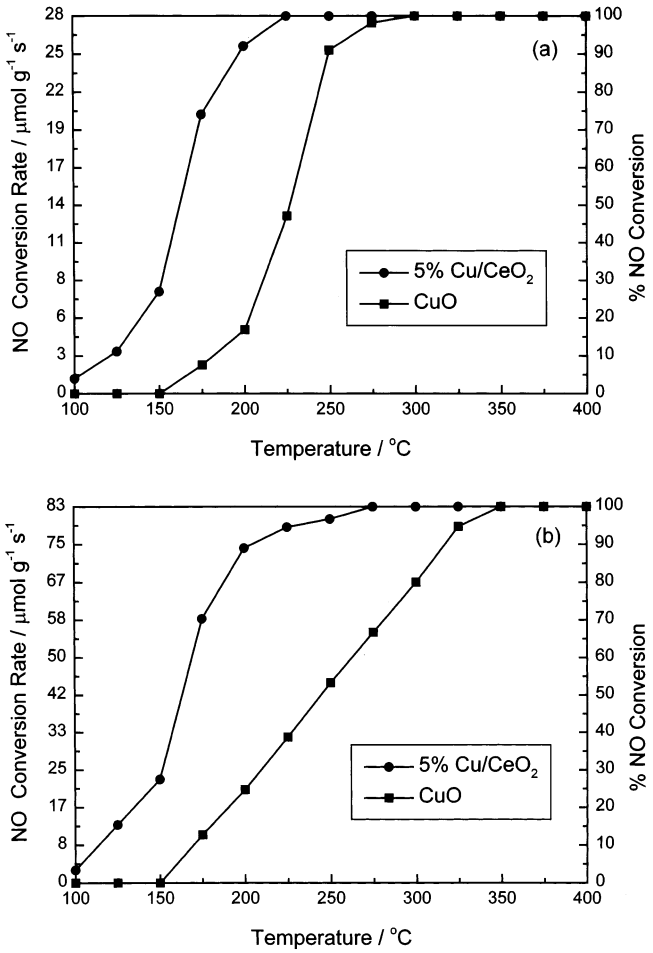

Figure 1. NO conversion rates for (a) NO + NH_3 and (b) NO + CO reactions over 5 atom % Cu/CeO_2 and CuO.

H_2 Uptake Studies. H_2 uptake (temperature programmed reduction) profiles over pure CeO_2, CuO, and 5 atom % Cu/CeO_2 as a function of temperature are shown in Figure 2. Over pure CeO_2, hydrogen uptake starts at about 300 °C, peaking at 550 °C, and the total hydrogen uptake obtained from the integrated area was 22 cm^3 g^{-1}, which is equivalent to an oxygen storage

(22) Newville, M.; Livins, P.; Yacobi, Y.; Rehr, J. J.; Stern, E. A. *Phys. Rev. B* **1993**, *47*, 14126.
(23) Pearson, W. P. In *Handbook of Lattice Spacings and Structures of Metals and Alloys*; Pergamon: New York, 1958.
(24) Zabinski, S. I.; Rehr, J. J.; Ankudinov, A.; Albers, R. C.; Eller, M. J. *Phys. Rev. B* **1995**, *52*, 2996.
(25) Stern, E. A.; Newville, M.; Ravel, B. D.; Yacoby, Y.; Haskel, D. *Physica B* **1995**, *208 and 209*, 117.
(26) Press, W. H.; Teulosky, S. A.; Vetterling, W. T.; Flannery, B. P. In *Numerical Recipies*; Cambridge University Press: New York, 1992.
(27) Bevington, P. R. In *Data Reduction and Error Analysis for Physical Sciences*; McGraw-Hill: New York, 1969.

capacity (OSC) of 11 $cm^3\ g^{-1}$. Even after five H_2/O_2 cycles over pure CeO_2, the decrease in OSC was less than 5%. The peak reduction temperature of CuO is about 325 °C (Figure 2). However, 5 atom % Cu/CeO_2 shows peaks at 75, 150, and 200 °C in addition to a peak at 600 °C. The first three peaks below 300 °C can be assigned to the reduction of Cu^{2+} ions in the CeO_2 matrix, whereas the peak at 600 °C can be attributed to the reduction of CeO_2 in comparison with pure CeO_2. A drastic decrease in the reduction temperature of Cu^{2+} ions in CeO_2 at 200 °C and below compared to 325 °C in pure CuO clearly demonstrates the absence of a CuO phase in 5 atom % Cu/CeO_2. Observation of three peaks at 75, 150, and 200 °C could be due to isolated Cu^{2+}, $-Cu^{2+}-O-Cu^{2+}-$ dimer and Cu^{2+} ions from the $-Cu^{2+}-O-Ce^{4+}-$ type of species present in the Cu/CeO_2 catalyst material. The relative intensities of these three peaks are 4, 11, and 85%, respectively. The amount of hydrogen under the peak at 200 °C is 13.5 $cm^3\ g^{-1}$ of 5 atom % Cu/CeO_2 catalyst, which is twice the amount of hydrogen required to reduce CuO to Cu^0, assuming all the Cu in 5 atom % Cu/CeO_2 is present as CuO. Excess hydrogen uptake than what is needed to reduce Cu^{2+} ions in the Cu/CeO_2 implies that some of Ce^{4+} ions gets reduced at low temperature. From XPS studies it has been confirmed that Cu^{2+} ions in 5 atom % Cu/CeO_2 get reduced to Cu^0. After hydrogen uptake up to 750 °C, the catalyst was cooled in O_2, temperature programmed reduction was repeated, and the profile obtained was the same as that shown in Figure 2. Further, even up to five H_2/O_2 cycles, the volume of hydrogen utilized did not decrease more than 2%. However, as is well-known, CuO reduced to Cu metal does not get oxidized to CuO in the presence of pure O_2. Indeed, there was no hydrogen uptake in the second cycle in the temperature programmed reduction of CuO. Therefore, Cu^{2+} ions in Cu/CeO_2 undergo a redox cycle, unlike the case for pure CuO. Thus, the H_2/O_2 cycling reaction in Cu/CeO_2 and CuO can be written as follows:

(i) For Cu/CeO_2

$$Cu^{2+} + 2Ce^{4+} + 2O^{2-} + 2H_2 \rightarrow Cu^0 + 2Ce^{3+} + 2H_2O \quad (1)$$

$$Cu^0 + 2Ce^{3+} + O_2 \rightarrow Cu^{2+} + 2Ce^{4+} + 2O^{2-} \quad (2)$$

(ii) For CuO

$$CuO + H_2 \rightarrow Cu^0 + H_2O \quad (3)$$

$$Cu^0 + O_2 \rightarrow \text{no reaction} \quad (4)$$

The hydrogen uptake study demonstrates that Cu^{2+} ion in Cu/CeO_2 can be reduced at a lower temperature than that for reduction of Cu^{2+} ion in CuO. Second, along with complete Cu^{2+} ion reduction to Cu^0, some of the Ce^{4+} seems to get reduced at the same temperature as that of reduction of Cu^{2+} ion in 5 atom % Cu/CeO_2. Both these points clearly suggest that Cu^{2+} ion is incorporated in the CeO_2 matrix and there is a chemical interaction between Cu^{2+} and CeO_2 which brings down the reduction temperature of Cu^{2+} ion as well as Ce^{4+} partially. This can be considered as the same promoting effect as that in the catalytic reaction over Cu/CeO_2 catalysts.

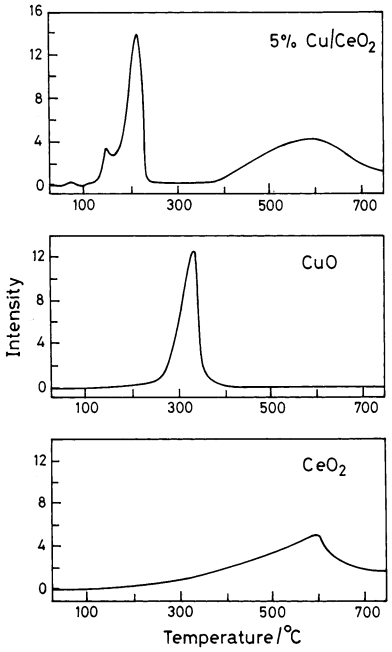

Figure 2. H_2 uptake over 5 atom % Cu/CeO_2, CuO, and pure CeO_2.

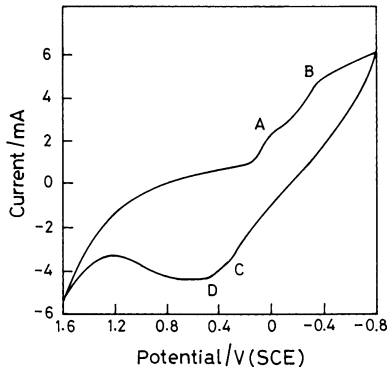

Figure 3. Cyclic voltammogram of Cu species in 5 atom % Cu/CeO_2 in 0.05 M Na_2SO_4 electrolyte at a scan rate of 50 mV s^{-1}.

CV Studies. The cyclic voltammogram of the 5 atom % Cu/CeO_2 electrode in 0.05 M Na_2SO_4 solution is shown in Figure 3. The voltammogram consists of two cathodic and two anodic peaks for the 5 atom % Cu/CeO_2 sample in the scan range 1.6 to −0.8 V/SCE. The Ce^{4+}/Ce^{3+} redox couple is not observed in the potential range studied. The first peak, labeled A, is attributed to the reduction of Cu(II) to Cu(I), and the second peak, B, is due to Cu(I) reduction to Cu(0) [see the figure]. The reduction potential values of $Cu^{2+} \rightarrow Cu^+$ and $Cu^+ \rightarrow Cu^0$ in CeO_2 matrix are −0.12 and −0.40 V, respectively, whereas the values corresponding to CuO electrodes are −0.28 and −0.50 V, respectively.[28] The oxidation potential values of $Cu^0 \rightarrow Cu^+$ (peak C) and $Cu^+ \rightarrow Cu^{2+}$ (peak D) in the CeO_2 substrate are +0.25 and +0.50 V, which are lower than those observed with the CuO (+0.36 and +0.60 V) electrode. Thus, the potential values indicate that the Cu species in the CeO_2 matrix require less energy to get reduced and oxidized than in the case of pure CuO.

(28) Xiao, J.; Villmure, G. *Clays Clay Miner.* **1998**, *46*, 195.

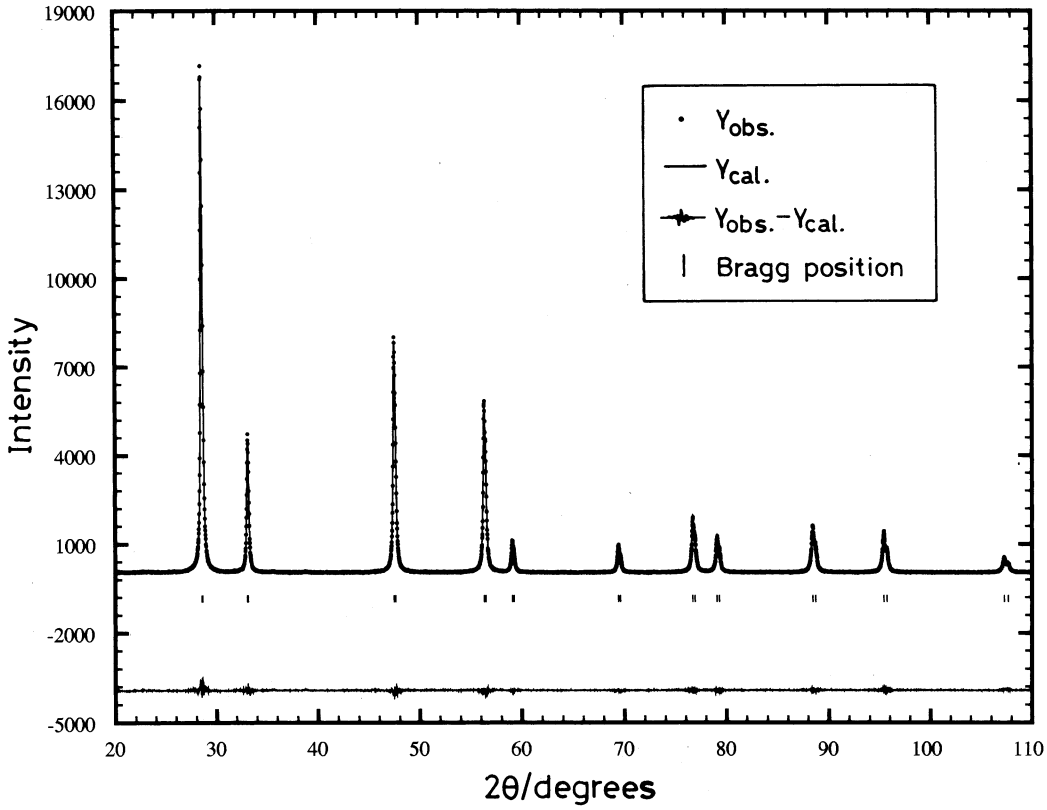

Figure 4. Observed, calculated, and difference XRD patterns of 5 atom % Cu/CeO_2.

XRD Studies. High-resolution X-ray diffraction data were collected for pure CeO_2 and 3 and 5 atom % Cu/CeO_2. Rietveld refinement of X-ray data was carried out, and in Figure 4, observed, calculated, and difference patterns of 5 atom % Cu/CeO_2 are given. The pattern is fitted to CeO_2 in the fluorite structure. The overall scale factor, background parameters, unit cell, shape, and isotropic thermal parameters were varied along with the occupancy. Diffraction lines due to CuO are not detected even when the 2θ region (30−50°) is expanded where CuO peaks are expected. Peaks due to Cu_2O are also not detected. XRD of 3 and 5 atom % Cu/CeO_2 samples heated at 800 °C for 24 h does not show CuO peaks. Pure CeO_2 prepared by the same combustion method crystallizes in the fluorite structure, and the refined lattice parameter is 5.411 28(25) Å. The R_{Bragg}, R_F, and R_p values are 0.91, 0.70, and 4.4%, respectively. The structure could be refined well with a total oxygen content of 1.934(11). Keeping the same Debye−Waller factors, the structure was refined for 3 and 5 atom % Cu/CeO_2. The lattice parameter a of 3 atom % Cu/CeO_2 is 5.410 95(10) Å with an oxygen content of 1.865(9). The R_{Bragg}, R_F, and R_p values are 1.38, 1.05, and 4.4%, respectively. In the case of 5 atom % Cu/CeO_2, the a value is 5.410 75(17) Å with an oxygen content of 1.843(10) and R_{Bragg}, R_F, and R_p were 1.41, 1.07, and 4.21%, respectively. The oxygen vacancy increased with the substitution of Cu^{2+} ion for the Ce^{4+} site, and accordingly, the compositions obtained from the fitting are $Ce_{0.97}Cu_{0.03}O_{1.87}$ and $Ce_{0.95}Cu_{0.05}O_{1.84}$. Because of the large difference in the scattering factor between cerium and oxygen, the absolute value of the oxygen occupancy is not reliable. However, from the high-quality data and fitting, a systematic decrease in oxygen content with increasing Cu^{2+} ion concentration is certainly dependable, indicating the presence of oxide ion deficiency. This observation is consistent with the recent study by Mamontov et al.[29] showing 3.5% oxygen vacancies in the nanocrystalline CeO_2. They have suggested that, in addition to oxygen vacancies in the tetrahedral site, Frenkel type oxygen vacancies in the octahedral site are stabilized in ceria−zirconia solid solution. If there is any substitution of Cu^{2+} ion in the Ce^{4+} site, the lattice parameter should decrease, as the ionic radius of Cu^{2+} (0.76 Å) is smaller than that of Ce^{4+} (1.01 Å). Indeed, a decrease in the lattice parameter from 5.411 28 Å in pure CeO_2 to 5.410 75 Å in 5 atom % Cu/CeO_2 confirms Cu^{2+} ion substitution in the CeO_2 matrix. Therefore, the XRD analysis shows that Cu^{2+} ions are incorporated with the CeO_2 lattice in the form of $Ce_{1-x}Cu_xO_{2-\delta}$ (x = 0.03, 0.05).

TEM Studies. TEM images of as-prepared pure CeO_2, 3 atom % Cu/CeO_2, and 5 atom % Cu/CeO_2 are shown in Figure 5. The average size of the CeO_2 crystallites in pure CeO_2 is 35 ± 5 nm, whereas it is 27 ± 5 nm in 3 and 5 atom % Cu/CeO_2, indicating a decrease in crystallite size of the Cu/CeO_2 catalyst. The morphology of theCeO_2 crystallites in all the cases is cubic. TEM images of the catalysts are similar to pure CeO_2 images, and there is no agglomerated CuO observed in the case of the Cu/CeO_2 crystallite surface. The ring type diffraction pattern of the catalysts could be indexed to polycrystalline CeO_2 in the fluorite structure (Figure 5d), and no line or even diffraction spots corresponding to any of the oxides of Cu is

(29) Mamontov, E.; Egami, T.; Brezny, R.; Koranne, K.; Tyagi, S. *J. Phys. Chem. B* **2000**, *104*, 11110.

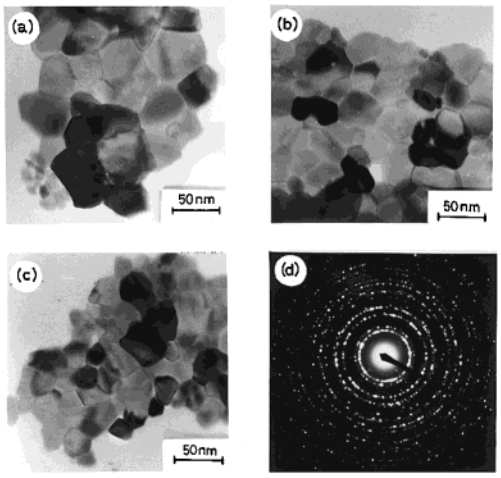

Figure 5. TEM of (a) CeO_2, (b) 3 atom % Cu/CeO_2, and (c) 5 atom % Cu/CeO_2 and (d) electron diffraction pattern of 5 atom % Cu/CeO_2.

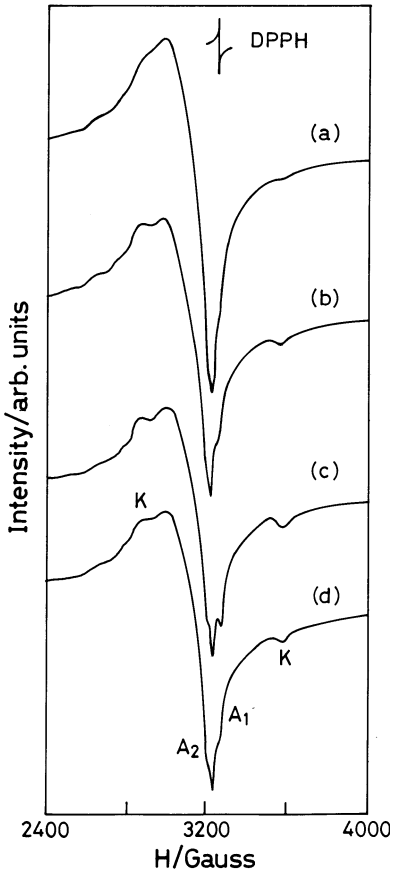

Figure 6. EPR spectra of 5 atom % Cu/CeO_2: (a) of freshly prepared sample; (b) after heat treatment at 600 °C for 12 h; (c) after NO + NH_3 and (d) NO + CO reactions.

detected. Therefore, TEM studies suggest that CuO is not separated out from the CeO_2 support. A decrease in the average crystallite sizes in Cu/CeO_2 compared to pure CeO_2 may be due to Cu^{2+} ions coming to the surface (as can be seen from XPS studies), hindering the growth of CeO_2 crystallites.

EPR Studies. EPR spectra of 5 atom % Cu/CeO_2 catalyst at different conditions are shown in Figure 6. The spectra are characteristics of a d^9-like species and can be assigned to Cu^{2+} ions. Each spectrum is composed of three signals which can be attributed to

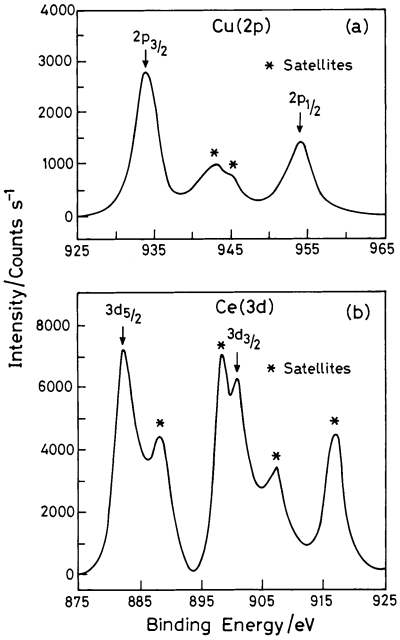

Figure 7. XPS of core level region of (a) Cu(2p) and (b) Ce(3d) in 5 atom % Cu/CeO_2.

monomers, dimers, and clusters of Cu^{2+}. The spectrum of the as-prepared catalyst contains Cu^{2+} species in a ceria matrix with EPR parameter values of $g_{\|} = 2.44$, $g_{\perp} = 2.09$, $A_{\|} = 125$ G, and $A_{\perp} = 20$ G. In each case, the magnitude of $g_{\|}$ is greater than that of $g_{\perp}$, indicating an unpaired electron occupying a $d_{x^2-y^2}$ orbital.[30] The A_1 and A_2 signals could be assigned to monomeric Cu^{2+} ions in CeO_2.[31,32] Further, signal K at 3000 and 3600 G in the spectra corresponds to $Cu^{2+}-Cu^{2+}$ ion pairs arising from the coupling between unpaired electrons of two Cu^{2+} ions. A weak signal (not shown in the figure) observed at half of the normal magnetic field (ca. 1600 G) corresponds to a forbidden transition ($\Delta m_s = 2$). On the other hand, the signal at the normal magnetic field corresponds to the allowed transition ($\Delta m_s = 1$). The interionic distance between the two Cu^{2+} ions forming the dimer has been estimated as 3.1 Å from the relation followed by Aboukaïs et al.[31]

There is no change in the characteristics of the EPR spectrum of the catalyst after heat treatment at 600 °C for 12 h. Formation of CuO crystallites on the catalyst surface due to heat treatment can decrease the effective intensity of the isolated Cu^{2+} signal. Indeed, there is no significant difference in the intensity of the Cu^{2+} signal in the heat-treated sample. However, the coupling constant slightly decreases. Thus, observation of an intense Cu^{2+} feature in the spectrum even after heat treatment suggests that CuO is not phase separated on heating of 5 atom % Cu/CeO_2. Further, the spectra of 5 atom % Cu/CeO_2 remain the same after NO + NH_3 and NO + CO reactions.

XPS Studies. The X-ray photoelectron spectrum of the core level regions of Cu(2p) in 5 atom % Cu/CeO_2 is given in Figure 7a. Cu($2p_{3/2,1/2}$) peaks are resolved into

(30) Cousin, R.; Capelle, S.; Abi-Aad, E.; Courcot, D.; Aboukaïs, A. *Chem. Mater.* **2001**, *13*, 3862.
(31) Aboukaïs, A.; Bennani, A.; Aïssi, C. F.; Wrobel, G.; Guelton, M.; Vedrine, J. C. *J. Chem. Soc., Faraday Trans.* **1992**, *88*, 615.
(32) Soria, J.; Conesa, J. C.; Martínez-Arias, A.; Coronado, J. M. *Solid State Ionics* **1993**, *63−65*, 755.

sets of spin−orbit doublets. Accordingly, the Cu($2p_{3/2,1/2}$) peaks at 934.0 and 953.8 eV with satellites at 9 eV below the main peak in 5 atom % Cu/CeO_2 can only be attributed to Cu in the +2 oxidation state. The satellite to main Cu peak (Cu $2p_{3/2}$) ratio (S/M) is 0.57 in this compound. The S/M value for CuO is 0.62. The S/M value varies from 0.37 to 0.47 in the case of Cu^{2+} ion in the square pyramidal position in $Bi_2Ca_{1-x}R_xSr_2$ $Cu_2O_{8+\delta}$ (R = Y, Yb).[33] Further, the S/M values are 0.55 and 0.85 for Cu^{2+} in the octahedral and tetrahedral sites of a cubic spinel.[34] Therefore, Cu^{2+} ion in this compound is not in tetrahedral coordination. Because the value is lower than that in CuO, Cu is not likely to be present in the CuO phase. The Ce(3d) peaks obtained from 5 atom % Cu/CeO_2 are shown in Figure 7b. The spectra with satellite features (marked in the figure) correspond to CeO_2 with Ce in the +4 oxidation state.[35]

The surface concentration ratio of Cu to Ce in Cu/CeO_2 has been estimated by the relation

$$\frac{X_{Cu}}{X_{Ce}} = \frac{I_{Cu}\sigma_{Ce}\lambda_{Ce}D_E(Ce)}{I_{Ce}\sigma_{Cu}\lambda_{Cu}D_E(Cu)} \quad (5)$$

where X, I, σ, λ, and D_E are the surface concentration, intensity, photoionization cross section, mean escape depth, and geometric factors, respectively. The integrated intensities of the Cu(2p) and Ce(3d) peaks have been taken into account to estimate the concentration. The photoionization cross section and mean escape depths have been obtained from the literature.[36,37] The surface concentration of Cu is 32% in 5 atom % Cu/CeO_2. The surface concentration of Cu in 10 atom % Cu/CeO_2 is 41%. Thus, the surface concentration of Cu is 4−6 times higher than what is taken in preparation, indicating surface segregation of Cu^{2+} ions on the CeO_2 surface.

X-ray photoelectron spectra of the 5 atom % Cu/CeO_2 sample after H_2 uptake measurement were also recorded to see if Cu^{2+} gets reduced to either Cu^+ or Cu^0. In the Cu(2p) spectrum of the reduced sample, the Cu($2p_{3/2}$) peak at 932.8 eV with no satellite peak indicates the presence of either Cu^+ or Cu^0 species. The Cu(L_3VV) Auger peak is observed at 917.6 eV in the same sample. If Cu^{2+} ion is reduced to the Cu^+ state, the Cu(L_3VV) Auger peak should have appeared at 916.0 eV. Thus, the Cu($2p_{3/2}$) peak at 932.8 eV, the absence of a satellite peak, and the observation of the Cu(L_3VV) Auger peak at 917.6 eV confirm the reduction of Cu^{2+} ion to Cu^0 on hydrogen reduction. Therefore, the XPS results justify the reactions given in eqs 1 and 2.

EXAFS Studies. In Figure 8a, Cu K-edge X-ray absorption near-edge structure (XANES) spectra of CuO, Cu_2O, and Cu metal are shown. The spectral features and characteristic of the compounds provide important clues to differentiate the chemical state and local symmetry of the Cu species.[38−41] A weak pre-edge peak ascribed to a dipole-forbidden electronic transition of 1s → 3d[42,43] appears at 8977 eV for the Cu^{2+} species in CuO. Cu^+ compounds, including Cu_2O, show an intense peak around 8983−8984 eV, attributable to dipole-allowed 1s → 4p electronic transitions.[42,43] To make XANES features more distinct, we have taken first derivatives of the XANES spectra. The main peak in the derivative spectra corresponds to the edge energy of each compound. The Cu^+ species in Cu_2O and the Cu^{2+} species in CuO show, respectively, a 1.5 and 3.5 eV shift in the main peak from that in Cu metal. In Figure 8b, the XANES spectra of the as-prepared 3 atom % Cu/CeO_2, 5 atom % Cu/CeO_2, and 10 atom % Cu/CeO_2 samples are presented. The near-edge structure of Cu in the catalytic compounds is also shifted by about 3.5 eV, indicating thereby Cu in the +2 state.

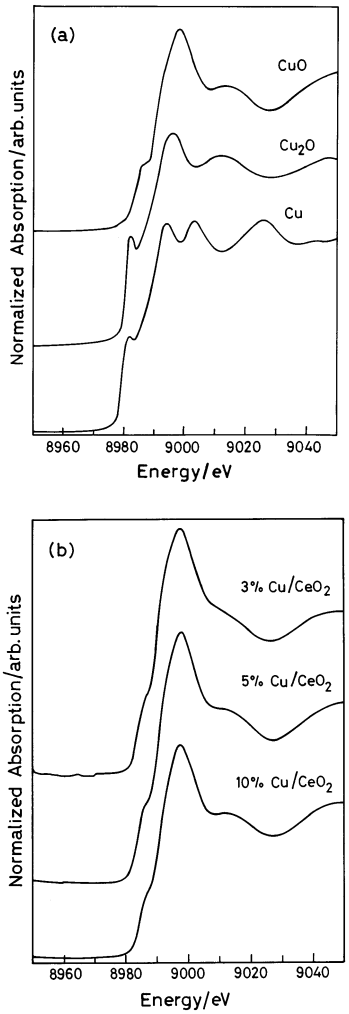

Figure 8. Normalized XANES spectra at the Cu K-edge of (a) CuO, Cu_2O, and Cu metal and (b) 3 atom % Cu/CeO_2, 5 atom % Cu/CeO_2, and 10 atom % Cu/CeO_2.

(33) Rao, C. N. R.; Rao, G. R.; Rajumon, M. K.; Sarma, D. D. *Phys. Rev. B* **1990**, *42*, 1026.
(34) Bechara, R.; Aboukaïs, A.; Bonnelle, J.-P. *J. Chem. Soc., Faraday Trans.* **1993**, *89*, 1257.
(35) Sarma, D. D.; Hegde, M. S.; Rao, C. N. R. *J. Chem. Soc., Faraday Trans. II* **1981**, *77*, 1509.
(36) Scofield, J. H. *J. Electron Spectrosc. Relat. Phenom.* **1976**, *8*, 129.
(37) Penn, D. R. *J. Electron Spectrosc. Relat. Phenom.* **1976**, *9*, 29.
(38) Grunet , W.; Hayes, N. W.; Joyner, R. W.; Shpiro, E. S.; Rafiq, M.; Siddiqui, H.; Baeva, G. W. *J. Phys. Chem.* **1994**, *98*, 10832.
(39) Kuroda, Y.; Yoshikawa, Y.; Konno, S.; Hamano, H.; Maeda, H.; Kumashiro, R.; Nagao, M. *J. Phys. Chem.* **1995**, *99*, 10621.
(40) Beutel, T.; Sarkany, J.; Lei, G. D.; Yan, J. Y.; Sachtler, W. M. H. *J. Phys. Chem.* **1996**, *100*, 845.
(41) Okamoto, Y.; Kubota, T.; Gotoh, H.; Ohto, Y.; Aritani, H.; Tanaka, T.; Yoshida, S. *J. Chem. Soc., Faraday Trans.* **1998**, *94*, 3473.
(42) Kau, L. S.; Spira-Solomon, D. J.; Penner-Hahn, J. E.; Hodgson, K. O.; Solomon, E. I. *J. Am. Chem. Soc.* **1987**, *109*, 6433.
(43) Kau, L. S.; Hodson, K. O.; Solomon, E. I. *J. Am. Chem. Soc.* **1989**, *111*, 7103.

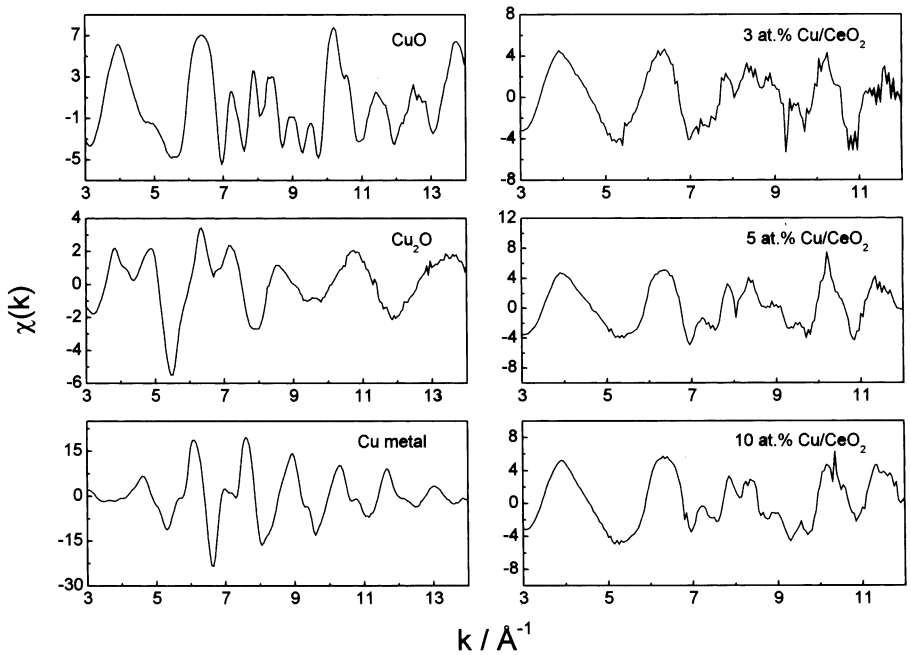

Figure 9. EXAFS functions of CuO, Cu_2O, Cu metal, 3 atom % Cu/CeO_2, 5 atom % Cu/CeO_2, and 10 atom % Cu/CeO_2.

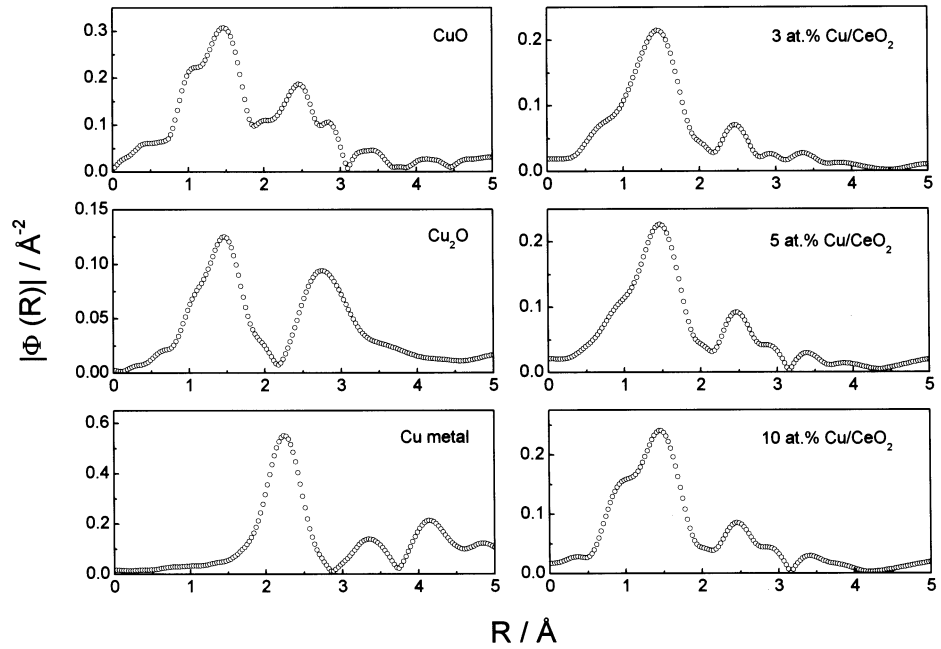

Figure 10. Fourier transforms of EXAFS functions for CuO, Cu_2O, Cu metal, 3 atom % Cu/CeO_2, 5 atom % Cu/CeO_2, and 10 atom % Cu/CeO_2.

The normalized EXAFS spectra of CuO, Cu_2O, Cu metal, and catalytic samples are presented in Figure 9. The EXAFS spectra of catalytic samples are also very similar to that of CuO. This indicates that the local environment around Cu ion in the catalysts seems to resemble that in CuO. The associated Fourier transforms (FTs) of $k^1\chi(k)$ for the reference materials and catalysts are shown in Figure 10. RSFs are not corrected for phase shifts, and so the observed peaks are shifted to lower *R*-values from the true interatomic distances. The fitting range for all the compounds is 1−4 Å. The *R*-factors are 0.01, 0.007, 0.01, 0.003, 0.006, and 0.006 for CuO, Cu_2O, Cu metal, 3 atom % Cu/CeO_2, 5 atom % Cu/CeO_2, and 10 atom % Cu/CeO_2, respectively. Structural parameters of the model compounds and the catalysts are given in Tables 1 and 2, respectively. The bond distances mentioned in the text and in the tables are phase-corrected values.

The coordination number and the bond distances of the model compounds CuO and Cu_2O and also the Cu metal agree well with those reported in the literature. CuO has been used as the primary model for fitting of all the catalytic compounds. This is because the XANES features which are the signature of the physicochemical environment of the central Cu ion are similar to those of CuO. The first coordination shell of Cu in the catalyst samples is at 1.96 Å, comparing well with that of Cu in CuO, but the average number of oxide ions around Cu^{2+} is 3 instead of 4 in CuO. In further shells of pure CuO, Cu is bonded to two O, four Cu, four Cu, and two Cu

Table 1. Structural Parameters of CuO, Cu_2O, and Cu Metal Foil Obtained from EXAFS Analysis

sample	shell	*N*	*R* (Å)	σ^2 (Å^{-2})
CuO	Cu−O	4.00	1.959 ± 0.004	0.005 ± 0.001
	Cu−O	2.00	2.784 ± 0.006	0.006 ± 0.001
	Cu−Cu	4.00	2.901 ± 0.006	0.010 ± 0.002
	Cu−Cu	4.00	3.072 ± 0.006	0.005 ± 0.001
	Cu−Cu	2.00	3.155 ± 0.004	0.001 ± 0.001
Cu_2O	Cu−O	2.00	1.858 ± 0.002	0.004 ± 0.001
	Cu−Cu	12.00	3.024 ± 0.003	0.022 ± 0.003
Cu metal	Cu−Cu	12.00	2.546 ± 0.004	0.009 ± 0.001
		6.00	3.601 ± 0.005	0.013 ± 0.003
		48.00	3.820 ± 0.005	0.016 ± 0.003
		48.00	4.347 ± 0.006	0.008 ± 0.001
		24.00	4.411 ± 0.006	0.015 ± 0.002
		48.00	4.752 ± 0.006	0.002 ± 0.001

Table 2. Structural Parameters for Cu/CeO_2 Catalysts Obtained from EXAFS Analysis

catalyst	shell	*N*	*R* (Å)	σ^2 (Å^{-2})
3 atom % Cu/CeO_2	Cu−O	3.14 ± 0.24	1.962 ± 0.002	0.005 ± 0.001
	Cu−Cu	2.04 ± 0.30	2.917 ± 0.006	0.007 ± 0.001
	Cu−Ce	6.16 ± 0.60	3.132 ± 0.006	0.020 ± 0.002
5 atom % Cu/CeO_2	Cu−O	3.15 ± 0.11	1.960 ± 0.004	0.005 ± 0.001
	Cu−Cu	4.63 ± 0.78	2.938 ± 0.003	0.010 ± 0.001
	Cu−Ce	3.37 ± 0.94	3.145 ± 0.005	0.009 ± 0.001
10 atom % Cu/CeO_2	Cu−O	3.15 ± 0.08	1.961 ± 0.002	0.004 ± 0.001
	Cu−Cu	6.08 ± 0.75	2.963 ± 0.002	0.014 ± 0.001
	Cu−Ce	1.92 ± 0.38	3.170 ± 0.005	0.005 ± 0.001

ions at 2.78, 2.90, 3.07, and 3.16 Å, respectively. However, distinct differences are seen in the second and third coordination shells of Cu in the catalysts compared to those in CuO. In the 3 atom % Cu/CeO_2 sample, the second coordination shell could be identified with Cu^{2+}–Cu^{2+} ion correlation at 2.92 Å with only two neighbors compared to four-coordinated Cu−Cu at 2.90 Å in pure CuO. However, the third shell at 3.13 Å with six atom coordination can not be accounted for using the CuO model. Therefore, we have chosen the solid solution model of the type $Ce_{1-x}Cu_xO_{2-\delta}$ to fit EXAFS data, as has been indicated by Rietveld refinement of XRD data of the catalyst samples. In pure CeO_2, the Ce−O−Ce angle is 109.5° and the corresponding Ce−O−Ce distance is 3.82 Å. If one of the Ce^{4+} ions is replaced by Cu^{2+} ion in CeO_2, the Cu−O−Ce distance would be 3.20 Å. The distance of 3.13 Å can only be accounted for by considering a Cu−O−Ce bond with bond angle of ∼89°. This is quite close to the Cu−O−Cu bond angle of 84.45° in CuO. This also agrees well with the observed XANES features of catalysts, which are very similar to those in XANES of CuO. Therefore, the EXAFS data have been fit with shells expected for Cu in the CuO lattice with an additional Cu−Ce interaction to account for the Cu−O−Ce correlation so that the second neighbors for Cu in Cu/CeO_2 could distribute between Cu and Ce neighbors, unlike in the case of only Cu in CuO. When the Cu concentration is increased to 5 atom %, coordination of the second and third shells is about 4 and 4 with distances of 2.94 and 3.15 Å, respectively. At 10 atom % Cu/CeO_2, the second and third shells are still at 2.96 and 3.17 Å but with 6 and 2 coordinations, respectively. Thus, as the concentration of Cu increases from 3 to 10 atom %, the coordination number of Cu^{2+} with Cu^{2+} ions increases from 2 to 6 and, correspondingly, the number of Ce^{4+} ions decreases from 6 to 2. The sum of the coordination numbers of the second and third shells remains at about 8. The Ce^{4+} ion in the CeO_2 lattice has 12 Ce neighbors in the second coordination. The surface Ce^{4+} ion will have 8 Ce^{4+} neighbors. If Cu substitution in the CeO_2 matrix is predominantly in the surface layers, as is indicated by XPS and the lower coordination number of O^{2-} ions in the first shell, 8 neighbors for Cu in the second shell in the catalyst can be justified. Further support of increasing Ce neighbors with decreasing Cu concentration comes from inverse transform spectra of reference materials and catalysts shown in Figure 11. In the CuO inverse spectrum (Figure 11), there is a small peak at about 5 Å^{-1} which is seen as a hump in 10 atom % Cu/CeO_2 (Figure 11), and it completely disappears in 3 atom % Cu/CeO_2.

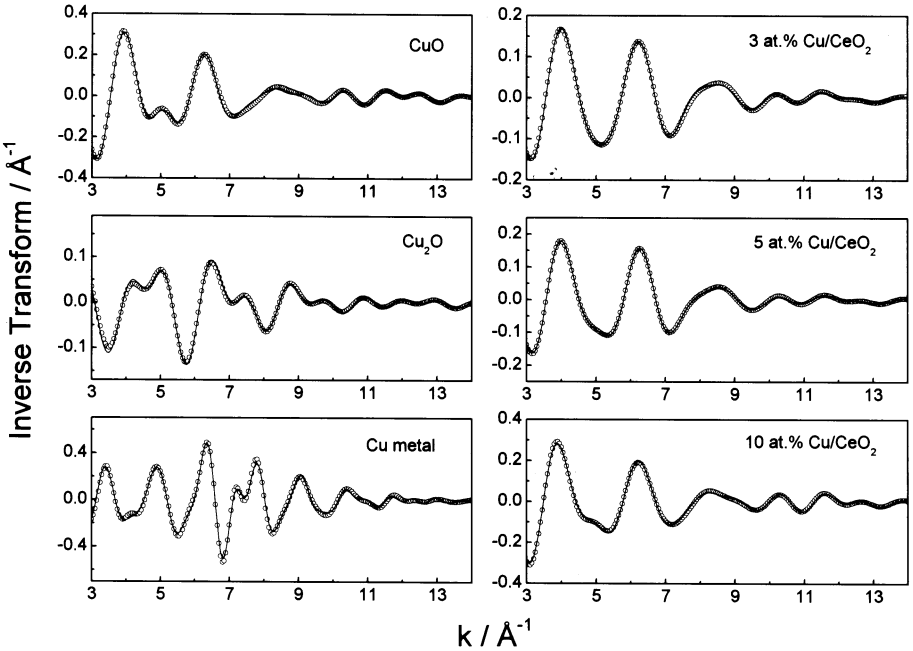

Figure 11. Inverse transforms of EXAFS functions of CuO, Cu_2O, Cu metal, 3 atom % Cu/CeO_2, 5 atom % Cu/CeO_2, and 10 atom % Cu/CeO_2 (continuous line indicates the fitted curve).

Discussion

The combustion method involves rapid heating of an aqueous solution containing stoichiometric amounts of corresponding metal salts and hydrazine based fuels. During the combustion, the temperature reached for a short period (30−60 s) is about 1000 °C, and it cooled to ∼300 °C in <1 min. Thus, the oxide formed at high temperature is quenched in the process. Evolution of a large amount of gases during the process is responsible for fine crystallite formation in the range 25−35 nm. In the conventional methods of Cu/CeO_2 preparation such as coprecipitation and impregnation, a precursor is heated for a long period of time, which may lead to separation of the thermodynamically stable phases CuO and CeO_2, and only some of the Cu^{2+} ions taken may get into the CeO_2 lattice. Thus, the above catalysts can have Cu^{2+} ion in the CeO_2 matrix.

In combustion synthesized Cu/CeO_2, either the Cu^{2+} ions should get separated into copper oxide species from the support or the Cu^{2+} ions should get incorporated into the ceria lattice. If there is an ionic substitution of Cu^{2+} ions for Ce^{4+} sites in the CeO_2 lattice, an oxide ion vacancy should be created in order to maintain the charge neutrality due to lower valent ionic substitution in addition to a decrease of the lattice parameter. Rietveld analysis of Cu/CeO_2 catalysts has clearly indicated the formation of $Ce_{1-x}Cu_xO_{2-\delta}$ with oxide ion vacancy. EPR and XPS studies have shown that Cu is present in the +2 state in Cu/CeO_2 catalysts. Further, the CuO phase could not be detected.

H_2 uptake over 5 atom % Cu/CeO_2 occurs at a lower temperature compared to that for pure CuO, indicating the promoting effect of CeO_2. Further, the H_2/O_2 cycle confirms the redox properties of Cu/CeO_2 which are not observed in CuO. Cyclic voltammetric studies demonstrate the direct redox behavior of Cu species in the CeO_2 matrix, which agrees well with the H_2 uptake experiment. It is observed that the redox potentials of Cu^{2+}/Cu^{+} and Cu^{+}/Cu^{0} couples in a CeO_2 matrix are lower than those in the CuO matrix. A decrease in Cu^{2+} ion reduction temperature in the temperature programmed reduction of Cu/CeO_2 compared to CuO correlates with the decrease in the redox potentials of Cu species in the CeO_2 matrix, providing direct evidence of the promoting action of CeO_2. This will result in a decrease in the energy required for the electron transfer during the redox type of catalytic reactions.

EXAFS studies of Cu/CeO_2 catalysts clearly indicate Cu^{2+} ion stabilization in Ce^{4+} sites in the form of $Ce_{1-x}Cu_xO_{2-\delta}$ solid solution. The EXAFS data analysis shows the oxygen vacancy around Cu^{2+} ions and a direct $-Cu^{2+}-O-Ce^{4+}-$ correlation at a distance of 3.15 ± 0.02 Å. In pure CeO_2, the oxygen ions are tetrahedrally coordinated to Ce^{4+} ions, giving a Ce−O−Ce angle of 109.5° and a Ce−Ce distance of 3.82 Å. Cu substitution in the Ce site must bring about a slight modification in the local environment around Cu. The respective Cu−O, Cu−Cu, and Cu−Ce correlations obtained from EXAFS analysis are 1.96, 2.94, and 3.15 Å and a Cu−O−Ce bond angle of 89°. It may be noted that the $Cu^{2+}-Cu^{2+}$ dimer distance calculated from the EPR study in 5 atom % Cu/CeO_2 is 3.1 Å, which is close to the value 2.94 Å obtained from EXAFS analysis. The $Cu^{2+}-Ce^{4+}$ correlation at 3.15 Å can only be possible via an oxide ion. Compared with the case of pure CuO, the coordination shells for Cu at 2.78 and 3.07 Å are not observed in the catalyst samples, suggesting Cu^{2+} in the Cu/CeO_2 catalyst is different from CuO. Even if one still persists with the CuO phase in catalysts by considering the 3.13 Å correlation in 3 atom % Cu/CeO_2 to be an average of correlations of four coordinated 3.07 and two coordinated 3.16 Å, then the change in coordination number of this shell in the 5 and 10% samples cannot be explained. The ionic radii of Cu^{2+}, O^{2-}, and Ce^{4+} are 0.76, 1.40, and 1.01 Å, respectively.[44] Accordingly, Cu^{2+}, O^{2-}, and Ce^{4+} ions with their real sizes in contact at 89° indeed give a $Cu^{2+}-Ce^{4+}$ distance of 3.15 Å, which is close to the 3.17 Å observed experimentally. The X-ray absorption spectroscopic study of 2−75 nm CeO_2 particles by Nachimuthu et al.[45] shows that for smaller particles (2−5 nm) the first coordination of Ce^{4+} is 6 (O^{2-}) and that for particles of ≥15 nm the coordination number is 8. Particle sizes of 3−10 atom % Cu/CeO_2 in our study are in the range 25−35 nm, and therefore, the first coordination of Ce^{4+} is expected to be 8 (Ce−O), following CeO_2 in the fluorite structure. It may be noted that Ce^{4+} ion on the CeO_2 surface has 4 coordination. If Cu^{2+} ions are substituted for surface Ce^{4+} in CeO_2, Cu^{2+} ion should have an average coordination number of 4. Our EXAFS study shows that the average coordination of Cu^{2+} is 3, suggesting oxide ion vacancies around Cu^{2+} ions on the surface of CeO_2. XPS study of a 4−6 times higher Cu^{2+} ion concentration on the surface indeed supports EXAFS data. The structural studies of Cu/CeO_2 in comparison with pure CeO_2 presented here demonstrate that, in the combustion synthesized Cu/CeO_2 catalysts, Cu^{2+} ions are incorporated into the CeO_2 nanoparticles in the form of $Ce_{1-x}Cu_xO_{2-\delta}$. Further Cu^{2+} ions are largely occupying the surface Ce^{4+} sites. For charge balancing, oxide ion vacancies are created.

Conclusions

The chemical state and local structure of Cu species in Cu/CeO_2 catalysts have been studied here. The salient findings in the present investigation are as follows.

(1) Catalytic reactions show that the Cu^{2+} species in the CeO_2 matrix is more active than Cu^{2+} in the CuO matrix.

(2) Rietveld refinement confirms the formation of $Ce_{1-x}Cu_xO_{2-\delta}$ in Cu/CeO_2 and the absence of a CuO phase.

(3) EPR and XPS studies show that Cu is in the +2 state in the Cu/CeO_2 catalyst.

(4) XANES of catalysts shows that a Cu^{2+} like species is present in the catalysts.

(5) Oxygen ion vacancy is created around the Cu^{2+} ion in the catalysts.

(6) The presence of bond distance at 3.15 Å in the Cu/CeO_2 catalyst corresponds to $Cu^{2+}-O^{2-}-Ce^{4+}$ correlation.

(7) Stabilization of Cu^{2+} ion in the Ce^{4+} site leads to the formation of a $Ce_{1-x}Cu_xO_{2-\delta}$ type of solid solution.

(44) Dikinson, S. K., Jr. In *Ionic, Covalent and Metallic Radii of the Chemical Elements*; Air Force Cambridge Research Laboratories: L. G. Hanscom Field, Bedford, MA, 1970.

(45) Nachimuthu, P.; Shih, W.-C.; Liu, R.-S.; Jang, L.-Y.; Chen, J.-M. *J. Solid State Chem.* **2000**, *149*, 408.

(8) The decrease of the redox potential of Cu^{2+} ions in the CeO_2 matrix is due to synergistic involvement of the Ce^{4+}/Ce^{3+} redox couple.

Acknowledgment. The Indian authors gratefully acknowledge the Department of Science and Technology (DST), Government of India, for financial support. Thanks are also due to the Japan Synchrotron Radiation Research Institute (SPring-8), Japan, for allotting beam time at the BL01B1 beam line and for local hospitality. We thank Dr. B. A. Dasannacharya, Director, IUC, Indore, for constant encouragement. Thanks are due to Mr. S. Mitra for cyclic voltammetry measurements.

CM0201706